Carbon Disulfide Reactions with Atomic Transition-Metal and Main-Group Cations: Gas-Phase Room-Temperature Kinetics and Periodicities in Reactivity

Ping Cheng, Gregory K. Koyanagi, and Diethard K. Bohme*

Department of Chemistry, Centre for Research in Mass Spectrometry and Centre for Research in Earth and Space Science, York University, Toronto, Ontario, Canada M3J 1P3

Received: December 5, 2005; In Final Form: January 13, 2006

The reactions of 46 atomic-metal cations with CS_2 have been investigated at room temperature using an inductively-coupled plasma/selected-ion flow tube (ICP/SIFT) tandem mass spectrometer. Rate coefficients and products were measured for the reactions of fourth-period atomic ions from K^+ to Se^+, of fifth-period atomic ions from Rb^+ to Te^+ (excluding Tc^+), and of sixth-period atomic ions from Cs^+ to Bi^+. Primary reaction channels were observed leading to S-atom transfer, CS_2 addition and, with Hg^+, electron transfer. S-atom transfer appears to be thermodynamically controlled and occurs exclusively, and with unit efficiency, in the reactions with most early transition-metal cations (Sc^+, Ti^+, Y^+, Zr^+, Nb^+, La^+, Hf^+, Ta^+, and W^+) and with several main-group cations (As^+, Sb^+) and less efficiently with Se^+, Re^+ and Os^+. Other ions, including most late transition and main-group metal cations, react with CS_2 with measurable rates mostly through CS_2 addition or not at all (K^+, Rb^+, Cs^+). Traces of excited states (<10%) were seen from an inspection of the observed product ions to be involved in the reactions with Mo^+, Te^+, Ba^+ and Au^+ and possibly Pt^+ and Ir^+. The primary products YS^+, ZrS^+, NbS^+, HfS^+, TaS^+, WS^+, ReS^+ and OsS^+ react further by S-atom transfer to form MS_2^+, and TaS_2^+ reacts further to form TaS_3^+. CS_2 addition occurs with the cations MCS_2^+, MS^+, MS_2^+, CS_2^+, and TaS_3^+ to form $M^+(CS_2)_n$ ($n \leq 4$), $MS^+(CS_2)_n$ ($n \leq 4$), $MS_2^+(CS_2)_n$ ($n \leq 3$), $(CS_2)_2^+$ and $TaS_3^+(CS_2)$. Up to four CS_2 molecules add sequentially to bare metal cations and monosulfide cations, and three to disulfide cations. Equilibrium constant measurements are reported that provide some insight into the standard free energy change for CS_2 ligation. Periodic variations in $\Delta G°$ are as expected from the variation in electrostatic attraction, which follows the trend in atomic-ion size and the trend in repulsion between the orbitals of the atomic cations and the occupied orbitals of CS_2.

1. Introduction

There is growing interest in the sulfur chemistry of metal centers, especially transition-metal atoms and cations, because of growing interests in catalytic and biological systems and in semiconductor materials containing sulfur.[1−3] Carbon disulfide is well suited for the study of metal−sulfur interactions because it can achieve several modes of coordination with one or more transition metals and can undergo a variety of insertion or disproportionation reactions.[4−6]As early as 1977, Huber et al.[7] showed that matrix reactions of CS_2 with Ni atoms at 10−12 K lead to the formation of $Ni(CS_2)_x$ ($x = 1-3$) adducts. Laser-ablated Co, Ni and Cu atoms and cations have been reacted with CS_2 during condensation in excess argon where they form metal and metal-cation adducts.[8] Similar investigations reported recently have demonstrated η^1 sulfur bonding in Ag(SCS) and Au(SCS) and the photochemically induced rearrangement into the inserted isomers SAgCS and SAuCS.[9] A theoretical study of the energy barrier for the insertion of V atoms into CS_2 also has appeared recently.[10] Also, the reaction mechanisms of the interactions of V and Cu atoms with CS_2 were investigated theoretically using density functional and coupled cluster calculations.[11]

Experimental investigations of gas-phase reactions of CS_2 with atomic cations have been restricted to those reported recently by the groups of Schwarz, using ion cyclotron resonance (FTICR) mass spectrometry, and Armentrout, using guided ion beam (GIB) mass spectrometry. After an early paper on the reaction with U^+,[12] these two groups reported experimental results, in a series of collaborative papers published between 1998 and 2002, for the reactions of U^+,[12] and the transition-metal cations Sc^+ and Ti^+,[13] V^+,[10,14] Cr^+ and Mn^+,[15] Fe^+,[16,17] Co^+,[16] Ni^+,[18] Cu^+,[18] and Zn^+.[18] The observed primary products generally were MS^+ and MCS^+. The dissertation of Kretzschmar provides a useful summary.[19] Jiang and Zhang[20] have provided a theoretical study of the potential-energy surface of the gas-phase reaction of Fe^+ with CS_2.

Here we report an extensive experimental survey of the room-temperature chemistry of 46 metal cations with CS_2 using ICP/SIFT tandem mass spectrometry in which all the atomic-metal cations are produced in an inductively coupled plasma (ICP) of argon at ca. 5500 K and then allowed to relax by radiation and collsions before reaction. Rate coefficients are measured for all the observed primary reactions and the sequential higher-order chemistry was monitored as well. The formation of higher-order CS_2 clusters was also assessed for the establishment of equilibrium, and this provides new measurements of the extent and strength of the binding of the CS_2 ligand to atomic-metal cations. Finally, because we have used the same technique previously to survey the reaction kinetics of the same 46 metal cations with the isovalent CO_2 molecule,[21] we provide a comparison of the kinetics for reactions with CS_2 with those of CO_2.

* Corresponding author. E-mail: dkbohme@yorku.ca. Phone: 416-736-2100, ext 66188. Fax: 416-736-5936.

10.1021/jp057078s CCC: $33.50
Published on Web 02/08/2006

2. Experimental Method

The experimental results reported here were obtained using the selected-ion flow tube (SIFT) tandem mass spectrometer described in detail elsewhere.[22,23] This instrument was recently modified to accept ions generated in an inductively coupled plasma (ICP) torch (ELAN series, Perkin-Elmer SCIEX) through an atmosphere/vacuum interface. The ICP ion source and interface have also been described previously.[24,25] Solutions containing the metal salt of interest with concentration of ca. 5 μg L^{-1} were peristaltically pumped via a nebulizer into the plasma. The nebulizer flow was adjusted to maximize the ion signal detected downstream of the flow tube. The sample solutions were prepared using atomic spectroscopy standard solutions commercially available from SPEX, Teknolab, J. T. Baker Chemical Co., Fisher Scientific Co., Perkin-Elmer and Alfa Products. Aliquots of standard solutions were diluted with highly purified water produced in the Millipore Milli-Qplus ultrapure water system. Single-isotope solutions were used for M^+ (m/z) = Ca^+ (44) and Se^+ (80). Readily soluble compounds of these metals were obtained from Oak Ridge National Laboratory (Isotope Business Office). The final concentrations were varied between 5 and 20 ppm to achieve suitable intensity of the resultant ion beam. Normally, a stabilizing agent was added to each solution to prevent precipitation. That was either HNO_3 or HCl for acid-stabilized salts or KOH for those base-stabilized.

Atomic ions emerge from the ICP at a nominal ion temperature of 5500 K with corresponding Boltzmann state distributions. These distributions have been derived from available optical spectra[26,27] and reported by us previously for the two electronic spin states with the highest population at 5500 K.[28] Energy levels as high as 3.7 eV (3×10^4 cm^{-1}) were included in the calculations. The calculations show that excited states of the main-group elemental cations except Ba^+ are high in energy and contribute little (never more than 10%) to the total ion population at 5500 K. The ground ^2S state of Ba^+ contributes 44% and the excited ^2D state 55% at 5500 K. The state distributions are more variable for the transition-metal cations. Excited states contribute 20% or less toward the populations of Cr^+, Mn^+, Ni^+, Cu^+, Zn^+, Rh^+, Pd^+, Ag^+, Cd^+ Re^+, Au^+ and Hg^+ and 50% or more toward the populations of Ti^+, Y^+, Zr^+, Nb^+, La^+ and Ir^+ with Sc^+, V^+, Fe^+, Co^+, Mo^+, Ru^+, Hf^+, Ta^+, W^+ and Pt^+ having intermediate distributions.

After extraction from the ICP, the plasma ions may experience both radiative electronic-state relaxation and collisional electronic-state relaxation. The latter may occur already with argon as the extracted plasma cools upon sampling and then by collisions with He atoms in the flow tube (ca. 4×10^5 collisions with He) prior to the reaction region, but the actual extent of electronic relaxation (either radiative or collisional) is not known and is difficult to assess. Almost all of the electronic states of the transition-metal ions have positive parity; electric dipole transitions between states of the same parity are forbidden (Laporte rule).[29] This means that radiative transitions between different states in metal cations can be achieved only by either magnetic dipole or electric quadrupole radiation. The probabilities for these transitions are very low,[30] and the resulting radiative lifetimes are of the order of seconds or larger. The time interval in the ICP/SIFT experiments between the exit of the ICP source and the entrance in the reaction region is ca. 20 ms and therefore no major modification of state distributions can occur in this time interval by forbidden radiative decay. That having been said, there were no indications of excited-state effects in our previous measurements of reactions of atomic cations derived from the same ICP source with N_2O, except with Pt^+.[28] The many collisions experienced by the atomic cations with the quite polarizable Ar atoms as they emerge from the ICP and the ca. 4×10^4 collisions with He atoms in the flow tube (the helium buffer gas pressure was 0.35 ± 0.01 Torr) appear to be sufficient to provide for the thermalization of the excited states and ensure that the atomic ions reach a translational temperature equal to the tube temperature of 295 ± 2 K prior to entering the reaction region. However, the exact extent of electronic relaxation is uncertain. Clues to the presence of excited electronic states of the atomic ions in the reaction region can be found in the product ions observed and the shape of the semilogarithmic decay of the reacting atomic ion upon addition of neutral reactant. Curvature will appear in the measured atomic-ion decay when the ground state and excited state react at different rates even when they give the same product ions. An excited-state effect cannot be seen when the products and reaction rates are the same for both the ground and excited states, but in this case the measured atomic-ion decay defines the ground-state kinetics. Our growing experience has shown that excited states can reveal themselves when the ground state of the atomic ion reacts only slowly by termolecular addition and excited states react rapidly in a bimolecular fashion.

CS_2 was introduced into the reaction region of the SIFT as a dilute (10%) mixture in helium. The CS_2 was obtained commercially and was of high purity (Matheson, Coleman & Bell, 99+%). Reaction rate coefficients were determined in the usual manner using pseudo first-order kinetics.[22,23] The rate coefficients for the primary and consecutive reactions reported herein have an absolute accuracy estimated to be $\pm$30%. When rate coefficients are reported as an upper limit ($\leq$), this indicates the statistical scatter in the data was significant compared to the slope of the data and an upper limit (based on the line of steepest slope through the data) is reported.

3. Results and Discussion

The reactions of CS_2 were measured with 46 atomic cations, including 29 transition-metal and 17 main-group cations. Both the primary and higher-order chemistries were monitored. Table 1 summarizes the measured rate coefficients, reaction efficiencies, observed primary products and product distributions and the observed higher-order product ions. The reaction efficiency is taken to be equal to the ratio k/k_c, where k is the experimentally measured rate coefficient and k_c is the capture or collision rate coefficient. k_c was computed using the algorithm of the modified variational transition-state/classical trajectory theory developed by Su and Chesnavich[31] with $\alpha(CS_2) = 8.74 \times 10^{-24}$ cm^3.[32]

The primary reactions exhibit a wide range in reactivity with measured rate coefficients from $<10^{-13}$ to 1.3×10^{-9} cm^3 $molecule^{-1}$ s^{-1}. Three reaction channels were observed and these are indicated in reaction 1. The bimolecular channels correspond

$$M^+ + CS_2 \rightarrow MS^+ + CS \quad (1a)$$

$$\rightarrow CS_2^+ + M \quad (1b)$$

$$\rightarrow M^+(CS_2) \quad (1c)$$

to S-atom transfer, reaction 1a, and electron transfer, reaction 1b. Electron transfer was observed only with Hg^+ (IE(Hg) = 10.44 eV).[32] Table 2 shows that all of the other metals investigated have ionization energies less than that of CS_2(IE(CS_2) = 10.0685 ± 0.0002 eV), so that electron transfer from

TABLE 1: Rate Coefficients (cm^3 molecule^{-1} s^{-1}), Reaction Efficiencies (k/k_c) and Higher-Order Product Ions Measured for Reactions of Atomic Ions M^+ with CS_2 in Helium at 0.35 ± 0.01 Torr and 295 ± 2 K[a]

M^+	k[b]	k_c[c]	k/k_c	primary products	PD[d]	higher-order product ions
K^+	$\leq 1.0 \times 10^{-12}$	1.35×10^{-9}	$\leq 7.4 \times 10^{-4}$			
Ca^+	1.0×10^{-11}	1.31×10^{-9}	7.5×10^{-3}	$Ca^+(CS_2)$	100	$Ca^+(CS_2)_{2-3}$
Sc^+	1.3×10^{-9}	1.31×10^{-9}	1.0	ScS^+	100	$ScS^+(CS_2)_{1-3}$
Ti^+	1.3×10^{-9}	1.28×10^{-9}	1.0	TiS^+	100	$TiS^+(CS_2)_{1-3}$
V^+	7.0×10^{-11}	1.26×10^{-9}	5.6×10^{-2}	$V^+(CS_2)$	100	$V^+(CS_2)_{2-3}$
Cr^+	1.0×10^{-11}	1.25×10^{-9}	8.1×10^{-3}	$Cr^+(CS_2)$	100	$Cr^+(CS_2)_2$
Mn^+	6.3×10^{-12}	1.23×10^{-9}	5.1×10^{-3}	$Mn^+(CS_2)$	100	$Mn^+(CS_2)_{2-3}$
Fe^+	3.6×10^{-11}	1.22×10^{-9}	3.0×10^{-2}	$Fe^+(CS_2)$	100	$Fe^+(CS_2)_2$
Co^+	8.9×10^{-11}	1.21×10^{-9}	7.4×10^{-2}	$Co^+(CS_2)$	100	$Co^+(CS_2)_{2-3}$
Ni^+	7.6×10^{-11}	1.21×10^{-9}	6.3×10^{-2}	$Ni^+(CS_2)$	100	$Ni^+(CS_2)_{2-3}$
Cu^+	5.7×10^{-11}	1.18×10^{-9}	4.8×10^{-2}	$Cu^+(CS_2)$	100	$Cu^+(CS_2)_{2-3}$
Zn^+	1.6×10^{-11}	1.18×10^{-9}	1.4×10^{-2}	$Zn^+(CS_2)$	100	$Zn^+(CS_2)_2$
Ga^+	3.7×10^{-12}	1.15×10^{-9}	3.2×10^{-3}	$Ga^+(CS_2)$	100	
Ge^+	7.6×10^{-11}	1.13×10^{-9}	6.7×10^{-2}	$Ge^+(CS_2)$	100	$Ge^+(CS_2)_2$
As^+	1.1×10^{-9}	1.13×10^{-9}	1.0	AsS^+	100	$AsS^+(CS_2)$
Se^+	3.3×10^{-10}	1.11×10^{-9}	0.30	SeS^+	85	$SeS^+(CS_2)$
				$Se^+(CS_2)$	15	
Rb^+	$\leq 1.0 \times 10^{-12}$	1.09×10^{-9}	$\leq 1.0 \times 10^{-3}$			
Sr^+	1.1×10^{-11}	1.18×10^{-9}	9.3×10^{-3}	$Sr^+(CS_2)$	100	$Sr^+(CS_2)_{2-3}$
Y^+	1.1×10^{-9}	1.08×10^{-9}	1.0	YS^+	100	$YS_2^+(CS_2)_{0-1}$
						$YS^+(CS_2)_{1-4}$
Zr^+	1.1×10^{-9}	1.1×10^{-9}	1.0	ZrS^+	100	$ZrS_2^+(CS_2)_{0-1}$
						$ZrS^+(CS_2)_{1-3}$
Nb^+	1.1×10^{-9}	1.07×10^{-9}	1.0	NbS^+	100	$NbS_2^+(CS_2)_{0-3}$
						$NbS^+(CS_2)_{1-2}$
Mo^+	1.0×10^{-10}	1.06×10^{-9}	9.4×10^{-2}	$Mo^+(CS_2)$	91	$Mo^+(CS_2)_{2-3}$
				MoS^+	9	$MoS^+(CS_2)$
Ru^+	9.9×10^{-11}	1.05×10^{-9}	9.4×10^{-2}	$Ru^+(CS_2)$	100	$Ru^+(CS_2)_{2-4}$
Rh^+	5.7×10^{-11}	1.05×10^{-9}	5.4×10^{-2}	$Rh^+(CS_2)$	100	$Rh^+(CS_2)_{2-4}$
Pd^+	4.5×10^{-11}	1.04×10^{-9}	4.3×10^{-2}	$Pd^+(CS_2)$	100	$Pd^+(CS_2)_{2-3}$
Ag^+	2.4×10^{-11}	1.04×10^{-9}	2.3×10^{-2}	$Ag^+(CS_2)$	100	$Ag^+(CS_2)_2$
Cd^+	7.5×10^{-12}	1.03×10^{-9}	7.3×10^{-3}	$Cd^+(CS_2)$	100	$Cd^+(CS_2)_2$
In^+	5.9×10^{-12}	1.02×10^{-9}	5.7×10^{-3}	$In^+(CS_2)$	100	
Sn^+	3.0×10^{-12}	1.02×10^{-9}	2.9×10^{-3}	$Sn^+(CS_2)$	100	$Sn^+(CS_2)_2$
Sb^+	1.0×10^{-9}	1.01×10^{-9}	1.0	SbS^+	100	$SbS^+(CS_2)$
Te^+	6.9×10^{-12}	1.0×10^{-9}	6.9×10^{-3}	$Te^+(CS_2)$	99	
				TeS^+	1	
Cs^+	$\leq 1.0 \times 10^{-12}$	9.96×10^{-10}	$\leq 1.0 \times 10^{-3}$			
Ba^+	4.4×10^{-11}	9.89×10^{-10}	4.4×10^{-2}	$Ba^+(CS_2)$	99	$Ba^+(CS_2)_{2-3}$
				BaS^+	1	$BaS^+(CS_2)$
La^+	9.9×10^{-10}	9.88×10^{-10}	1.0	LaS^+	100	$LaS^+(CS_2)_{1-3}$
Hf^+	9.6×10^{-10}	9.48×10^{-10}	1.0	HfS^+	100	$HfS_2^+(CS_2)_{0-2}$
						$HfS^+(CS_2)_{1-3}$
Ta^+	9.5×10^{-10}	9.48×10^{-10}	1.0	TaS^+	100	$TaS_2^+(CS_2)_{0-3}$
						$TaS_3^+(CS_2)_{0-1}$
						$TaS^+(CS_2)_{1-2}$
W^+	9.5×10^{-10}	9.44×10^{-10}	1.0	WS^+	100	$WS_2^+(CS_2)_{0-2}$
Re^+	2.7×10^{-10}	9.40×10^{-10}	0.28	ReS^+	88	$Re^+(CS_2)_2$
				$Re^+(CS_2)$	12	$ReS^+(CS_2)_{1-2}$
						$ReS_2^+(CS_2)_{0-1}$
Os^+	9.4×10^{-10}	9.38×10^{-9}	1.0	OsS^+	70	$OsS^+(CS_2)_{1-3}$
				$Os^+(CS_2)$	30	$OsS_2^+(CS_2)_{0-1}$
						$Os^+(CS_2)_{2-4}$
Ir^+	7.9×10^{-10}	9.38×10^{-10}	0.84	$Ir^+(CS_2)$	85	$Ir^+(CS_2)_{2-4}$
				IrS^+	15	$IrS^+(CS_2)_{1-3}$
Pt^+	3.5×10^{-10}	9.36×10^{-10}	0.36	$Pt^+(CS_2)$	95	$Pt^+(CS_2)_{2-3}$
				PtS^+	5	$PtS^+(CS_2)_{1-2}$
Au^+	1.7×10^{-10}	9.35×10^{-10}	0.18	$Au^+(CS_2)$	91	$Au^+(CS_2)_2$
				AuS^+	1	$AuS^+(CS_2)$
				$AuCS^+$	4	$AuCS^+(CS_2)$
				CS_2^+	4	$(CS_2)_2^+$
Hg^+	9.3×10^{-10}	9.32×10^{-10}	1.0	CS_2^+	100	$(CS_2)_2^+$
Tl^+	4.7×10^{-12}	9.30×10^{-10}	5.0×10^{-3}	$Tl^+(CS_2)$	100	
Pb^+	5.4×10^{-12}	9.28×10^{-10}	5.8×10^{-3}	$Pb^+(CS_2)$	100	
Bi^+	6.5×10^{-12}	9.27×10^{-10}	7.0×10^{-3}	$Bi^+(CS_2)$	100	

[a] The atomic ions are ordered according to period in the periodic table. Primary products and product distributions (PD) are also included. [b] Measured reaction rate coefficient with an estimated accuracy of ±30%. [c] Calculated collision rate coefficient (see text). [d] PD = product distribution expressed as a percentage, with an estimated accuracy of ±5%.

TABLE 2: S-Atom Affinities, $D_0(M^+-S)$ (kcal mol^{-1}), and Ionization Energies, IE(M) (eV), for Some Atomic Cations

M^+	$SA(M^+)$[a]	IE(M)[b]	M^+	$SA(M^+)$[a]	IE(M)[b]	M^+	$SA(M^+)$	IE(M)[b]
K^+		4.34	Rb^+		4.18	Cs^+		3.89
Ca^+		6.11	Sr^+		5.69	Ba^+		5.21
Sc^+	114.6 ± 1.2	6.56	Y^+	126.6 ± 1.9	6.22	La^+	124 ± 12[d]	5.58
Ti^+	109.3 ± 1.7	6.83	Zr^+	127.3 ± 5.0	6.63	Hf^+		6.83
V^+	87.2 ± 2.4	6.75	Nb^+	127.1 ± 2.4	6.76	Ta^+		7.55
Cr^+	61.9 ± 3.8	6.77	Mo^+	84.8 ± 1.2	7.09	W^+		7.86
Mn^+	58.0 ± 5.5	7.43	Tc^+			Re^+		7.83
Fe^+	70.9 ± 1.0	7.90	Ru^+	68.8 ± 1.4	7.36	Os^+		8.43
Co^+	68.1 ± 2.1	7.88	Rh^+	54.0 ± 3.1	7.46	Ir^+		8.97
Ni^+	56.6 ± 0.96	7.64	Pd^+	47.1 ± 1.4	8.34	Pt^+		8.96
Cu^+	47.8.4 ± 3.3	7.72	Ag^+	29.4 ± 3.1	7.58	Au^+		9.23
Zn^+	47.3 ± 2.9	9.39	Cd^+		8.99	Hg^+		10.44
Ga^+		6.00	In^+	40 ± 12[c]	5.79	Tl^+		6.11
Ge^+	86 ± 14[c]	7.90	Sn^+	77[c]	7.34	Pb^+	55 ± 12[c]	7.42
As^+		9.79	Sb^+		8.61	Bi^+	48 ± 12[c]	7.29
Se^+	102 ± 5[c]	9.75	Te^+		9.01			

[a] Unless indicated otherwise, values for $SA(M^+)$ are taken from the review of P. B. Armentrout.[35] [b] Taken from ref 32. [c] Determined from $\Delta H_f°(MS^+)$, $\Delta H_f°(M^+)$, and $\Delta H_f°(S)$ found in ref 34. [d] Determined from IE(La) found in ref 32 and from IE(LaS) and D(La−S) found in ref 36.

CS_2 to these M^+ cations is endothermic.[32] The addition reactions (1c) are expected to be termolecular with He buffer gas atoms acting as the stabilizing third body (rate coefficients were not measured as a function of He pressure). C-atom transfer to form metal carbide, MC^+, cations was not observed. In the experiments with Au^+ we observed CS transfer to form $AuCS^+$, but this can be attributed to an excited-state reaction as discussed below. Figure 1 displays the data in Table 1, with excited-state effects (see below) removed, and shows the trends in overall reaction efficiencies and product distributions across the periodic table for the reactions of 46 metal cations with CS_2.

Of the first-row transition-metal cations investigated by Armentrout, Schwarz et al.,[10,13−18] only Sc^+ and Ti^+ were found to react with CS_2 in an exothermic fashion at thermal energy. The FTICR measurements provided rate coefficients for S-atom transfer of $(7.7 \pm 1.5) \times 10^{-10}$ and $(7.6 \pm 1.5) \times 10^{-10}$ cm^3 molecule^{-1} s^{-1} for Sc^+ and Ti^+ respectively, and a reaction efficiency of 0.60 ± 0.12 for *both* metal cations.[13] Our values are slightly higher and identical for the reactions of both cations: $k = (1.3 \pm 0.4) \times 10^{-9}$ cm^3 molecule^{-1} s^{-1} and $k/k_c = 1.0 \pm 0.3$ for both Sc^+ and Ti^+ at 295 K.

Exclusive S-atom abstraction was observed with 11 of the 46 atomic cations that were investigated. These are the early transition-metal cations (group 3, Sc^+, Y^+, and La^+; group 4, Ti^+, Zr^+, and Hf^+; group 5, Nb^+ and Ta^+) as well as W^+ and the main-group cations As^+ and Sb^+. All of these reactions were observed to be fast, $k > 9 \times 10^{-10}$ cm^3 molecule^{-1} s^{-1} and the efficiencies for S-atom transfer were all equal to 1.0.

Exclusive or competing CS_2 addition according to reaction 1c was observed for 31 other late transition-metal and main-group atomic cations. Many of the addition reactions are quite fast with measured effective bimolecular rate coefficients for CS_2 addition are $>10^{-11}$ cm^3 molecule^{-1} s^{-1} but some (first row cations) are immeasurably slow with $k < 10^{-13}$ cm^3 molecule^{-1} s^{-1} at 0.35 ± 0.01 Torr of He and 295 ± 2 K.

The reactions with the third-row transition-metal cations Re^+, Os^+, Ir^+ and Pt^+ and with Se^+ displayed both addition and S-atom transfer with the proportion of adduct formation increasing across the row.

Water impurities in the helium buffer gas also were observed to react with some of the bare metal cations, and with some primary and higher-order product ions. The early bare transition-metal cations can react with water by O-atom transfer to form

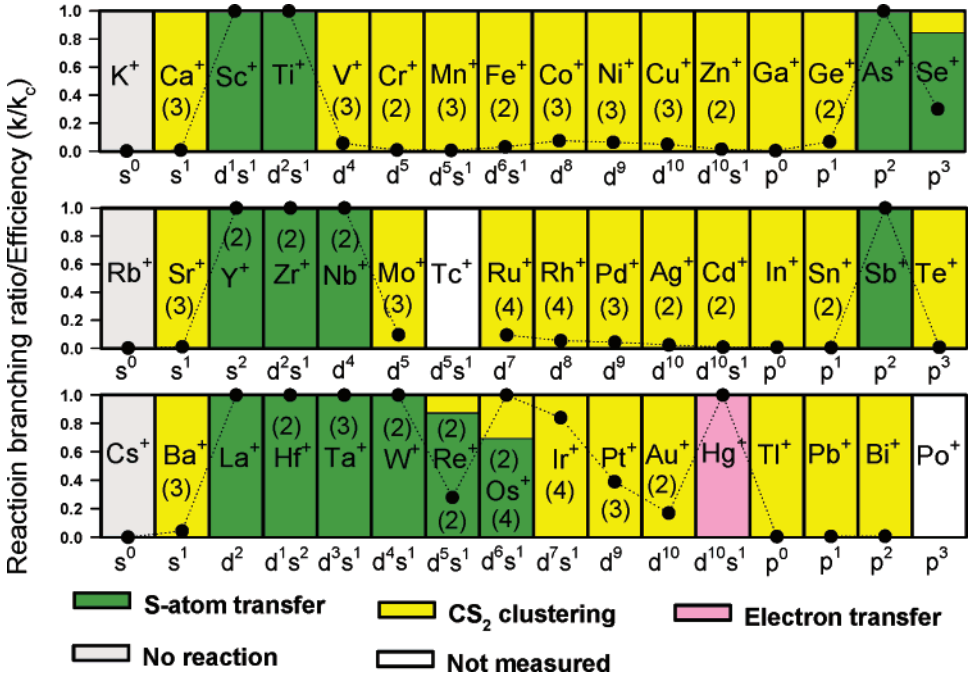

Figure 1. Periodic variations observed in the reaction efficiencies, k/k_c (represented as solid circles), for reactions of ground-state atomic cations with CS_2. k represents the measured reaction rate coefficient and k_c is the calculated collision rate coefficient Also indicated are the observed reaction channels and the electronic configurations of the atomic cations in their ground states. Small excited-state effects in the reactions of Mo^+ (9%), Te^+ (1%), Ba^+ (1%), Au^+ (9%), Ir^+ and Pt^+, (see text) are not shown. The numbers in parentheses given above the element indicate the number of sequential S-atom transfer reactions that were observed, and those given below the element indicate the number of sequential CS_2 addition reactions that were observed.

MO^+.[33] The MO^+ cation can react with CS_2 by S-atom transfer to form MOS^+ and this was apparent with Ta^+. Water can also add to $M^+(CS_2)_n$, $MS^+(CS_2)_n$ and $MS_2^+(CS_2)_n$ or switch with one of the CS_2 ligands.

3.1. Fourth-Period Atomic Ions. Only S-atom transfer and CS_2 addition were observed as primary reaction channels with fourth-period atomic cations. S-atom transfer occurs with the very early transition-metal cations Sc^+ and Ti^+ and the main-group cations As^+ and Se^+. Some (15%) CS_2 addition was observed to compete with the S-atom transfer to Se^+. Only CS_2 addition was observed with all the other cations in the fourth period.

Secondary and higher-order CS_2 addition occur with both MS^+ and $M^+(CS_2)$ ions as is seen in Figure 2 which presents data for Sc^+, Ti^+, Co^+ and As^+. Higher-order CS_2 addition according to reaction 2 was observed for the first row cations

$$M^+(CS_2)_n + CS_2 \rightarrow M^+(CS_2)_{n+1} \qquad (2)$$

$M^+ = Ca^+$ ($n = 1-2$), V^+ ($n = 1-2$), Cr^+ ($n = 1$), Mn^+ ($n = 1-2$), Fe^+ ($n = 1$), Co^+ ($n = 1-2$), Ni^+ ($n = 1-2$), Cu^+ ($n = 1-2$), Zn^+ ($n = 1$), and Ge^+ ($n = 1$). The Ga^+ cation only added one CS_2 molecule and K^+ none in the range of CS_2 flow that was investigated. Reaction 3 was observed for $MS^+ = ScS^+$

$$MS^+(CS_2)_n + CS_2 \rightarrow MS^+(CS_2)_{n+1} \qquad (3)$$

($n = 0-2$), TiS^+ ($n = 0-2$), AsS^+ ($n = 0$) and SeS^+ ($n = 0$) in the range of CS_2 flow that was investigated. The results with Co^+ show an example of the occurrence of a switching reaction in which the H_2O impurity in the He buffer gas switches with a CS_2 molecule in $Co^+(CS_2)_2$ according to reaction 4. Because

$$Co^+(CS_2)_2 + H_2O \rightarrow Co^+(CS_2)(H_2O) + CS_2 \qquad (4)$$

the amount of H_2O in He is constant, the observed rise in $Co^+(CS_2)(H_2O)$ is parallel to that of $Co^+(CS_2)_2$. The direct addition of impurity H_2O to $Co^+(CS_2)$ is not competitive in the formation of $Co^+(CS_2)(H_2O)$ because it occurs in a termolecular fashion with a much lower effective bimolecular rate.

3.2. Fifth-Period Atomic Cations. S-atom transfer and CS_2 addition also predominates in the reactions of the fifth-period metal cations with CS_2. S-atom transfer was observed with Y^+, Zr^+, Nb^+ and Sb^+, and CS_2 addition with Sr^+, Mo^+, Ru^+, Rh^+, Pd^+, Ag^+, Cd^+, In^+, Sn^+ and Te^+. The Rb^+ cation was found to be nonreactive with $k < 10^{-13}$ cm^3 molecule^{-1} s^{-1}.

Figure 3 displays the primary and higher-order chemistry observed with Y^+, Zr^+, Nb^+ and Rh^+. The occurrence of secondary S-atom transfer according to reaction 5 is seen in

$$MS^+ + CS_2 \rightarrow MS_2^+ + CS \qquad (5)$$

Figure 1 for the early transition-metal cations of $M^+ = Y^+$, Zr^+, and Nb^+. Secondary and higher-order CS_2 addition is observed with M^+, MS^+ and MS_2^+. Reactions of type (2) were seen with $M^+ = Sr^+$ ($n = 1-2$), Mo^+ ($n = 1-2$), Ru^+ ($n = 1-3$), Rh^+ ($n = 1-3$), Pd^+ ($n = 1-2$), Ag^+ ($n = 1$), Cd^+ ($n = 1$), and Sn^+ ($n = 1$). Reactions of type (3) were observed with $MS^+ = YS^+$ ($n = 0-3$), ZrS^+ ($n = 0-2$), NbS^+ ($n = 0-1$), and SbS^+ ($n = 0$). Reactions of type (6) were observed with

$$MS_2^+(CS_2)_n + CS_2 \rightarrow MS_2^+(CS_2)_{n+1} \qquad (6)$$

$MS_2^+ = YS_2^+$ ($n = 0$), ZrS_2^+ ($n = 0$), and NbS_2^+ ($n = 0-2$) and can be seen in Figure 3. Water switching reactions of type (4) are seen in Figure 3 to lead to the formation of $YS^+(H_2O)$ and $ZrS^+(H_2O)$ and the mixed cluster ions $YS^+(CS_2)(H_2O)$, $ZrS^+(CS_2)(H_2O)$, $YS^+(CS_2)_2(H_2O)$ and $NbS_2^+(CS_2)(H_2O)$.

3.3. Sixth-Period Atomic Cations. The S-atom transfer and CS_2 addition are still the dominant reactions with the sixth-period atomic cations. S-atom transfer was observed with La^+,

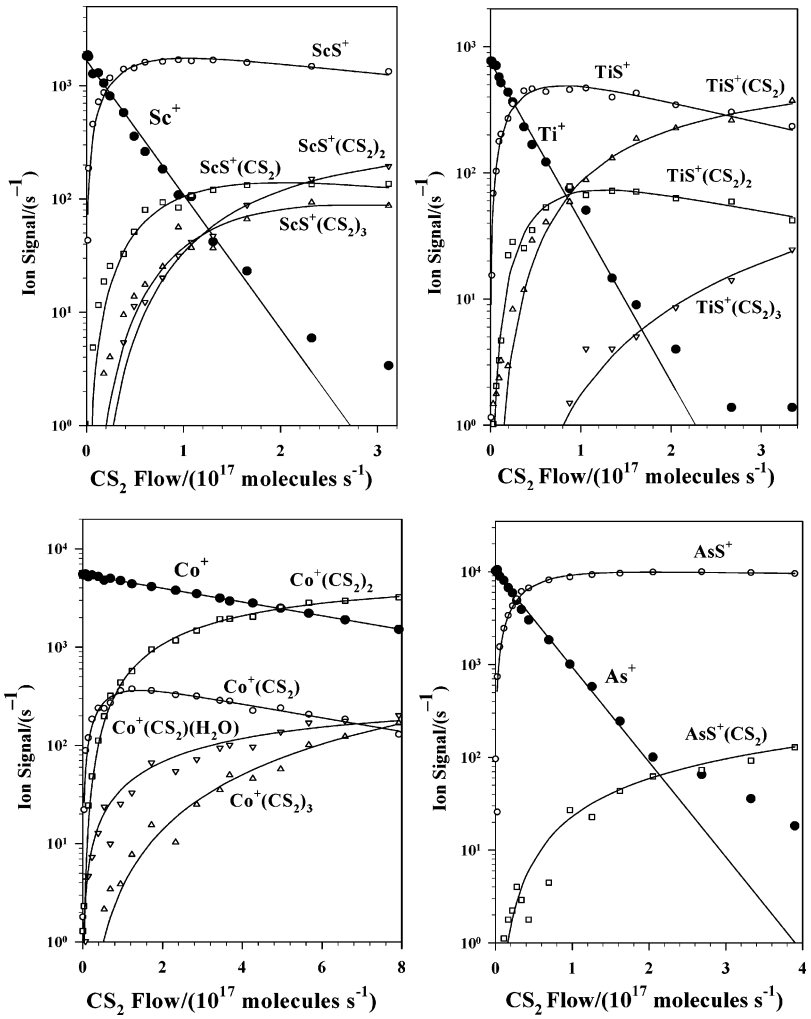

Figure 2. Composite of ICP/SIFT results for the reactions of the fourth-period atomic cations Sc^+, Ti^+, Co^+ and As^+ with CS_2 in helium buffer gas at 0.35 ± 0.01 Torr and 295 ± 2 K.

Hf^+, Ta^+ and W^+, and CS_2 addition with Ba^+, Ir^+, Pt^+, Au^+, Tl^+, Pb^+ and Bi^+. S-atom transfer was observed to compete with CS_2 addition with Re^+ and Os^+. Cs^+ was found to be totally nonreactive whereas CS_2 was seen to transfer an electron to Hg^+.

Figure 4 displays the primary and higher-order chemistry observed with Ta^+, W^+, Re^+ and Hg^+. The Ta^+ data show the sequential transfer of three S atoms leading ultimately to the formation of the trisulfide tantalum cation according to reaction 7. MS_3^+ was not observed with any other atomic cation.

$$TaS_2^+ + CS_2 \rightarrow TaS_3^+ + CS \qquad (7)$$

Secondary and higher-order CS_2 addition is observed with M^+, MS^+, MS_2^+ and MS_3^+. Reactions of type (2) were seen with $M^+ = Ba^+$ ($n = 1-2$), Re^+ ($n = 1$), Os^+ ($n = 1-3$), Ir^+ ($n = 1-3$), Pt^+ ($n = 1-2$) and Au^+ ($n = 1$). Reactions of type (3) were observed with $MS^+ = HfS^+$ ($n = 0-2$), TaS^+ ($n = 0-1$) and OsS^+ ($n = 0-2$). Reactions of type (6) were observed with $MS_2^+ = HfS_2^+$ ($n = 0-1$), TaS_2^+ ($n = 0-2$), WS_2^+($n = 0-1$) and OsS_2^+ ($n = 0$). TaS_3^+ was observed to add one CS_2 molecule according to reaction 8 as can be seen in Figure 4.

$$TaS_3^+ + CS_2 \rightarrow TaS_3^+(CS_2) \qquad (8)$$

Figure 4 also shows that the electron-transfer product, CS_2^+, adds a CS_2 molecule to form the CS_2 dimer cation. The appearance of $WS_2^+(H_2O)$ can be assigned to the switching reaction of $WS_2^+(CS_2)$ with H_2O impurity in the helium buffer gas and this suggests that $D(WS_2^+-H_2O) > D(WS_2^+-CS_2)$.

3.4. Thermodynamics for S-Atom Transfer. The affinity of CS for S atoms is quite high, SA(CS) = 103.77 ± 0.92 kcal mol^{-1}.[34] Available S-atom affinities for atomic cations are listed in Table 2 and these are known for only 25 of the 46 atomic cations that were investigated. Of these, six (the early transition-metal cations Sc^+, Ti^+, Y^+, Zr^+, Nb^+ and La^+) have $SA(M^+) > SA(CS)$ within experimental uncertainty and so are expected on thermodynamic grounds to abstract an S atom from CS_2. All have been observed to do so with unit efficiency, $k/k_c = 1.0$!

$SA(Se^+) = 102 \pm 5$ kcal mol^{-1}, which is slightly lower than SA(CS), and this may explain the reduced efficiency of 0.30 and the competition of S-atom transfer (85%) with CS_2 addition (15%) measured for the reaction with Se^+.

The S-atom affinities of As^+ as well as the third-row atomic cations Hf^+, Ta^+, and W^+, with which S-atom transfer was observed to proceed with unit efficiency, are not known. All of these cations should therefore have S-atom affinities > SA(CS) = 104 kcal mol^{-1}. The same should apply to Se^+, Re^+ and Os^+, all of which react predominantly by S-atom transfer with branching ratios (85%, 88% and 70%, respectively much larger than the maximum population of excited states emerging from the ICP (7.1%, 12.1% and an unknown percentage, respectively).[28]

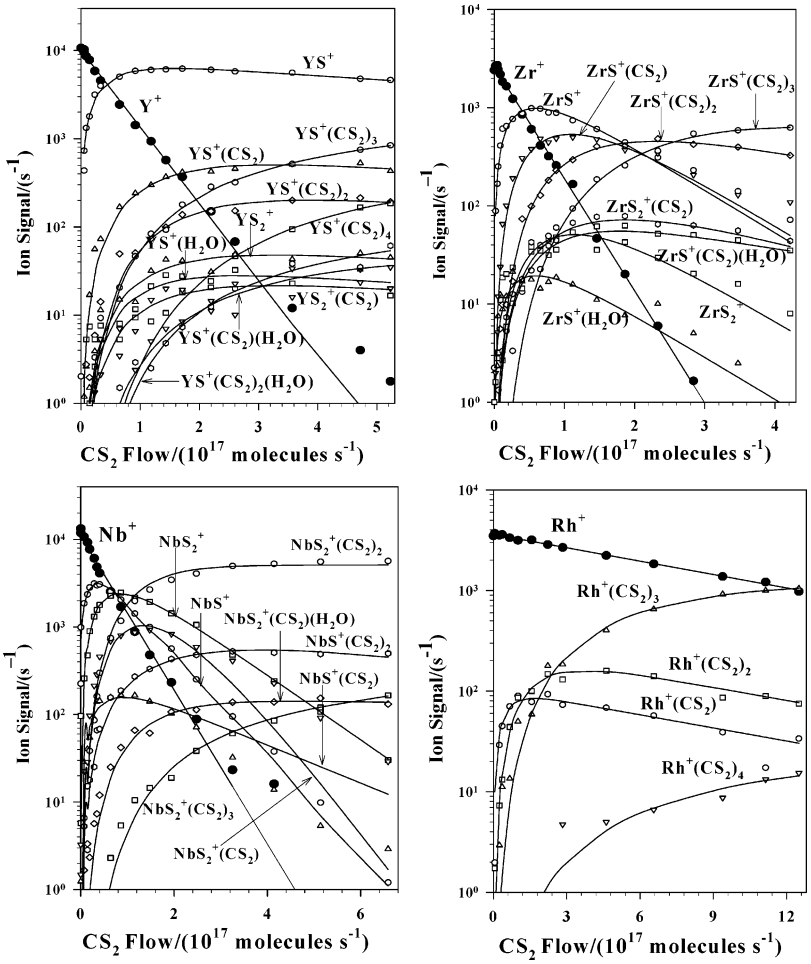

Figure 3. Composite of ICP/SIFT results for the reactions of the fifth-period atomic cations Y^+, Zr^+, Nb^+ and Rh^+ with CS_2 in helium buffer gas at 0.35 ± 0.01 Torr and 295 ± 2 K.

Figure 5 displays the overall dependence of the efficiency of S-atom transfer on the known S-atom affinities of metal cations. It is clear from this Figure that those ground-state ions known to have SA(M^+) ≥ SA(CS) react with CS_2 by S-atom transfer with high efficiency, and those known to have SA(M^+) < SA(CS) react with CS_2 just by CS_2 addition and with a lower efficiency.

3.5. Role of Excited States. The reactions of Pt^+ and Ir^+ also exhibit S-atom transfer, but these are minor channels (5 and 15%, respectively) compared to the observed CS_2 addition, and they arise most likely from excited states that have populations in the ICP source at 5500 K as high as 38 and 56%, respectively.[28] The S-atom affinities of ground-state Pt^+ and Ir^+ are not known, but they should be less than 100 kcal mol^{-1} judging from the low S-atom affinities of the other atomic cations in the same groups.

The case is clearer for ground-state Mo^+, which has a known S-atom affinity of 84.8 ± 1.2 kcal mol^{-1} (see Table 1) and with which S-atom transfer is clearly endothermic (by 19 ± 2 kcal mol^{-1}). The measured percentage for the S-atom transfer channel observed with Mo^+ is 9%, and this must clearly arise from excited Mo^{+*}. Excited Mo^+(^{6}D) has a population at 5500 K determined to be 12.74% for energies between 1.46 and 1.67 eV that are sufficiently high to overcome the endothermicity for S-atom transfer from CS_2. A similar situation is very likely to apply to the formation of the monosulfide cations of Te^+, Ba^+ and Au^+ that were observed to be produced each with a branching ratio of 1%. The experiments with Au^+ also revealed the formation of $AuCS^+$ and CS_2^+ (IE(CS_2) = 10.07 eV). Electron transfer is endothermic with ground-state Au^+(^{1}S) and this may well also be the case for S-atom and CS transfer. The excited Au^+(^{3}D) state, which accounts for about 16% of the total Au^+ cations within the ICP, has an energy of about 1.84−3.44 eV. Such energy is sufficient to drive the electron transfer (45%) and probably also S-atom (16%) and CS transfer (39%) where the % refers to the % of the total products attributed to excited-state chemistry.

3.6. Addition of CS_2. Most of the late transition-metal cations and the main-group cations were observed to react with CS_2 by addition. Almost exclusive (≥85%) CS_2 addition was observed with Ca^+, V^+, Cr^+, Mn^+, Fe^+, Co^+, Ni^+, Cu^+, Zn^+, Ga^+, Ge^+, Sr^+, Mo^+, Ru^+, Rh^+, Pd^+, Ag^+, Cd^+, In^+, Sn^+, Te^+, Ba^+, Ir^+, Pt^+, Au^+, Tl^+, Pb^+ and Bi^+. The reaction efficiencies for these reactions are in the range of 0.0029 (Sn^+) to 0.71 (Ir^+). S-atom transfer with what is expected to be excited-state cations was the main competing channel in the reactions with Mo^+ (9%), Te^+ (1%), Ba^+ (1%), Ir^+ (15%) and Pt^+ (5%). CS_2 addition competes with major S-atom transfer in the reactions with Se^+, Re^+, and Os^+ with efficiencies of 0.045, 0.034, and 0.30, respectively.

The CS_2 addition efficiency for late transition-metal cations (group 7−12) is very low. In the first row, from group 7 to group 9, the reactions show an increased reactivity, and from group 10 to group 12, the reactions exhibit a reduced reactivity. The reaction efficiency first increases from 0.0051 (Mn^+) to 0.074 (Co^+) and then reduces to 0.014 (Zn^+). In the second row, from group 8 to group 12, the reactions show a reduced reactivity and the reaction efficiency reduces from 0.094 (Ru^+)

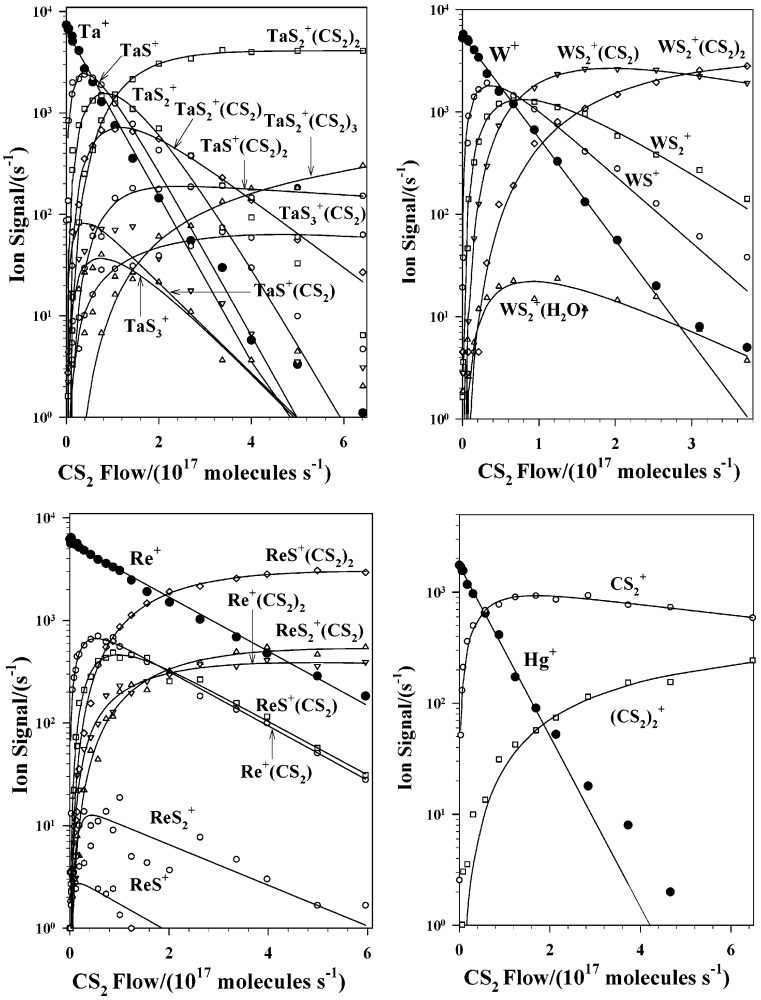

Figure 4. Composite of ICP/SIFT results for the reactions of the fifth-period atomic cations Ta^+, W^+, Re^+ and Hg^+ with CS_2 in helium buffer gas at 0.35 ± 0.01 Torr and 295 ± 2 K.

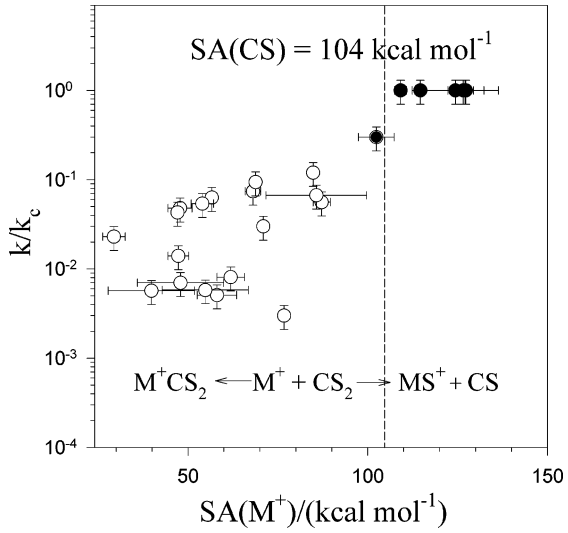

Figure 5. Dependence of the reaction efficiency, k/k_c, on the S-atom affinity, SA, of the atomic cation. k represents the measured reaction rate coefficient and k_c is the calculated collision rate coefficient (see Table 1). Open circles correspond to CS_2 addition, and filled circles designate S-atom transfer. Reactions on the right of the dashed line are exothermic for S-atom transfer, and those on the left are endothermic.

to 0.0057 (In^+). In the third row, the CS_2 addition efficiency is below 0.01 for Tl^+, Pb^+ and Bi^+ but larger than 0.18 for Re^+, Os^+, Ir^+, Pt^+ and Au^+. The main-group cations also add CS_2 very slowly with low efficiencies, the highest being that with Ge^+ (0.067).

The abnormally high efficiencies ($\geq$0.18) for the CS_2 addition reactions with the third-row transition-metal cations Re^+, Os^+, Ir^+, Pt^+ and Au^+ probably arise from abnormally strong bonding in the adduct ions that are formed. Unfortunately, little is known about the strengths of these particular interactions. Our equilibrium constant measurements for the addition reactions provide some support for strong bonding, as will be discussed later.

3.7. Secondary and Higher-Order Reactions. Some of the primary product ions were observed to continue to react with CS_2 to produce the higher-order product ions listed in Table 1. Secondary and higher-order rate coefficients were determined by fitting the profiles of these ions monitored as a function of the flow of CS_2.

Sequential S-Atom Transfer. A second S-atom abstraction, reaction 6, was observed with the early transition-metal sulfide cations YS^+, ZrS^+, NbS^+, HfS^+, TaS^+, WS^+, ReS^+ and OsS^+. The rate coefficients measured for these reactions are summarized in Table 3 along with calculated reaction efficiencies. The reactions of NbS^+, TaS^+ and WS^+ are the most efficient, $k/k_c > 0.8$, and those with YS^+ and ZrS^+ the least, $0.006 < k/k_c < 0.05$. S-atom affinities for these transition-metal sulfide cations are not currently available, but they must be larger than $D(S-CS) = 104 \pm 1$ kcal mol^{-1} if they are all exothermic.

TABLE 3: Measured Rate Coefficients for S-Atom Transfer from CS_2 to Metal Monosulfide Cations in Helium at 0.35 ± 0.01 Torr and 295 ± 2 K

reaction	k^a	$k_c{}^b$	k/k_c
$YS^+ + CS_2 \rightarrow YS_2^+ + CS$	6.0×10^{-12}	1.00×10^{-9}	6.0×10^{-3}
$ZrS^+ + CS_2 \rightarrow ZrS_2^+ + CS$	4.2×10^{-11}	1.00×10^{-9}	4.2×10^{-2}
$NbS^+ + CS_2 \rightarrow NbS_2^+ + CS$	8.3×10^{-10}	1.00×10^{-9}	0.83
$HfS^+ + CS_2 \rightarrow HfS_2^+ + CS$	8.6×10^{-11}	9.21×10^{-10}	9.3×10^{-2}
$TaS^+ + CS_2 \rightarrow TaS_2^+ + CS$	8.5×10^{-10}	9.20×10^{-10}	0.92
$WS^+ + CS_2 \rightarrow WS_2^+ + CS$	8.4×10^{-10}	9.19×10^{-10}	0.91
$ReS^+ + CS_2 \rightarrow ReS_2^+ + CS$	3.7×10^{-10}	9.18×10^{-10}	0.40
$OsS^+ + CS_2 \rightarrow OsS_2^+ + CS$	8.7×10^{-11}	9.15×10^{-10}	9.5×10^{-2}

[a] Measured reaction rate coefficient in units of cm^3 $molecule^{-1}$ s^{-1} with an estimated accuracy of ±30%. [b] Calculated capture rate coefficient (see text).

TABLE 4: Measured Reaction Rate Coefficients k (cm^3 $molecule^{-1}$ s^{-1}) and Reaction Efficiencies (k/k_c) for Sequential CS_2 Addition to Atomic Ions M^+ at 0.35 ± 0.01 Torr and 295 ± 2 K

	$M^+(CS_2)$		$M^+(CS_2)_2$		$M^+(CS_2)_3$	
M^+	k^a	$k/k_c{}^b$	k^a	$k/k_c{}^b$	k^a	$k/k_c{}^b$
Ca^+	1.0×10^{-11}	7.5×10^{-3}	1.6×10^{-10}	0.16	1.0×10^{-10}	0.11
V^+	7.0×10^{-11}	5.6×10^{-2}	7.0×10^{-10}	0.70		
Cr^+	1.0×10^{-11}	8.1×10^{-3}	6.0×10^{-10}	0.60		
Mn^+	6.3×10^{-12}	5.1×10^{-3}	1.1×10^{-10}	0.11		
Fe^+	3.6×10^{-11}	3.0×10^{-2}	1.1×10^{-9}	1.1		
Co^+	8.9×10^{-11}	7.4×10^{-2}	9.0×10^{-10}	0.90	9.0×10^{-12}	9.7×10^{-3}
Ni^+	7.6×10^{-11}	6.3×10^{-2}	1.0×10^{-9}	1.0	1.5×10^{-10}	0.16
Cu^+	5.7×10^{-11}	4.8×10^{-2}	1.0×10^{-9}	1.0		
Zn^+	1.6×10^{-11}	1.4×10^{-2}	1.6×10^{-11}	1.6×10^{-2}		
Ga^+	3.7×10^{-12}	3.2×10^{-3}				
Ge^+	7.6×10^{-11}	6.7×10^{-2}	7.0×10^{-12}	7.1×10^{-3}		
Se^+	5.0×10^{-11}	4.5×10^{-2}				
Sr^+	1.1×10^{-11}	9.3×10^{-3}	4.7×10^{-11}	4.9×10^{-2}	1.0×10^{-11}	1.1×10^{-2}
Mo^+	1.0×10^{-10}	9.4×10^{-2}	1.1×10^{-9}	1.1	5.0×10^{-11}	5.5×10^{-2}
Ru^+	9.9×10^{-11}	9.4×10^{-2}	1.0×10^{-9}	1.0	7.8×10^{-10}	0.86
Rh^+	5.7×10^{-11}	5.4×10^{-2}	1.0×10^{-9}	1.0	4.3×10^{-10}	0.47
Pd^+	4.5×10^{-11}	4.3×10^{-2}	7.3×10^{-10}	0.77	3.0×10^{-10}	0.33
Ag^+	2.4×10^{-11}	2.3×10^{-2}	3.1×10^{-10}	0.33		
Cd^+	7.5×10^{-12}	7.3×10^{-3}	7.4×10^{-12}	7.9×10^{-3}		
In^+	4.2×10^{-12}	5.7×10^{-3}				
Sn^+	3.0×10^{-12}	2.9×10^{-3}				
Te^+	6.9×10^{-12}	6.9×10^{-3}				
Ba^+	4.4×10^{-11}	4.4×10^{-2}	6.9×10^{-12}	7.8×10^{-3}		
Re^+	4.1×10^{-11}	4.2×10^{-2}	1.0×10^{-9}	1.1		
Os^+	2.8×10^{-10}	0.30	3.4×10^{-10}	0.38		
Ir^+	6.7×10^{-10}	0.71	1.0×10^{-9}	1.1	4.0×10^{-11}	4.5×10^{-2}
Pt^+	3.3×10^{-10}	0.35	1.0×10^{-9}	1.1	4.0×10^{-11}	4.5×10^{-2}
Au^+	1.7×10^{-10}	0.18	1.1×10^{-9}	1.2		
Tl^+	4.7×10^{-12}	5.0×10^{-3}				
Pb^+	5.4×10^{-12}	5.8×10^{-3}				
Bi^+	6.5×10^{-12}	7.0×10^{-3}				

[a] Measured reaction rate coefficient with an estimated accuracy of ± 50%. [b] k_c is the calculated collision rate coefficient (see text).

The structure of the MS_2^+ ions formed in reaction 6 are also uncertain, as at least three isomers are possible: the cyclic form, c-MS_2^+, and two acyclic forms, SMS^+ and MSS^+. Our multicollision technique,[37] which involves simply raising the potential of the sampling nose cone, did not yield bond cleavage for MS_2^+ and so did not provide bond connectivity information. Structures and electronic states of MS_2^+ cations with M = V, Fe, and Mo have been calculated using the hybrid functional B3LYP.[17,38] Cyclic *side-on* isomers were found to be the global minima of FeS_2^+ ($^6A_1$ ground state) and VS_2^+ ($^3A_1$ ground state), whereas the inserted species $SMoS^+$ ($^2A_1$) was seen to be the most stable species of MoS_2^+. Although energy onsets for the formation of these disulfide ions were observed in the guided-ion beam experiments,[17,38] none of these particular disulfide ions were observed to be formed at the thermal energies of our experiments. Both of these experimental results imply that the formation of these disulfide ions is endothermic.

TABLE 5: Measured Reaction Rate Coefficients k (cm^3 $molecule^{-1}$ s^{-1}) and Reaction Efficiencies (k/k_c) for Sequential CS_2 Addition to MS^+ and MS_2^+ at 0.35 ± 0.01 Torr and 295 ± 2 K

	$MS_n^+(CS_2)$		$MS_n^+(CS_2)_2$		$MS_n^+(CS_2)_3$	
MS_n^+	k^a	$k/k_c{}^b$	k^a	$k/k_c{}^b$	k^a	$k/k_c{}^b$
ScS^+	9.6×10^{-11}	0.10	7.2×10^{-10}	0.79	8.2×10^{-10}	0.92
TiS^+	1.4×10^{-10}	0.14	1.0×10^{-9}	1.1		
AsS^+	1.0×10^{-11}	1.2×10^{-2}				
SeS^+	5.0×10^{-11}	5.3×10^{-2}				
YS^+	5.0×10^{-11}	5.3×10^{-2}	5.0×10^{-10}	0.56	8.0×10^{-10}	0.91
ZrS^+	4.0×10^{-10}	0.43	8.0×10^{-10}	0.89	2.0×10^{-10}	0.23
NbS^+	8.0×10^{-11}	8.8×10^{-2}	9.0×10^{-10}	1.0		
NbS_2^+	8.0×10^{-10}	0.88	9.0×10^{-10}	1.0		
SbS^+	1.6×10^{-11}	1.7×10^{-2}				
LaS^+	2.5×10^{-11}	2.7×10^{-2}	1.8×10^{-10}	0.20	2.0×10^{-10}	0.23
HfS^+	4.8×10^{-10}	0.52	9.0×10^{-10}	1.0		
TaS^+	9.5×10^{-11}	0.11	9.0×10^{-10}	1.0		
TaS_2^+	7.0×10^{-10}	0.80				
WS_2^+	4.0×10^{-10}	0.45	2.3×10^{-10}	0.26		
OsS^+	7.8×10^{-10}	0.88	9.0×10^{-10}	1.0		

[a] Measured reaction rate coefficient with an estimated accuracy of ±50%. [b] k_c is the calculated collision rate coefficient (see text).

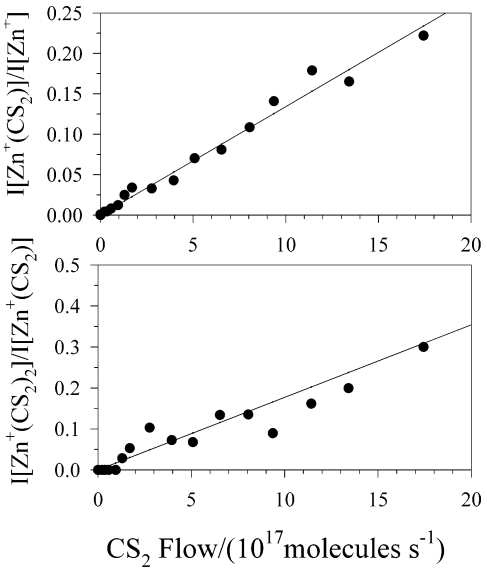

Figure 6. Variations observed in the ion signal ratio of $I[Zn(CS_2)_{n+1}]/I[Zn(CS_2)_n]$ ($n = 0, 1$) for the sequential addition of CS_2 to Zn^+ with the flow rate of CS_2 molecules.

A third S-atom abstraction, reaction 7, also was observed, but only with Ta^+. No other higher-order S-atom abstractions were seen in our experiments.

Sequential CS_2 Addition. Most of the product ions $(CS_2)^+$, MS^+, MS_2^+, CS_2^+, TaS_3^+ and $AuCS^+$ were observed to continue to react with CS_2 by addition resulting in the formation of the cluster ions $M^+(CS_2)_n$ ($n \leq 4$), $MS^+(CS_2)_n$ ($n \leq 4$), $MS_2^+(CS_2)_n$ ($n \leq 3$), $(CS_2)_2^+$, $TaS_3^+(CS_2)$ and $AuCS^+(CS_2)$.

Kinetic results obtained for the sequential addition of CS_2 to atomic M^+ cations are summarized in Table 4. Those for the sequential addition of CS_2 to MS^+ and MS_2^+ cations are summarized in Table 5. Note the significant increase in the efficiency of CS_2 addition to atomic cations after the first addition of CS_2. This increase could be entirely due to the increased number of degrees of freedom in the intermediate cation that needs to be collisionally stabilized to form a stable adduct ion, although an increase in the binding energy may also

TABLE 6: Equilibrium Constants, *K* (Standard State = 1 atm), Measured for Sequential CS_2 Addition to Atomic Cations at 295 ± 2 K[a]

	K (Δ*G*°)		
M^+	$M^+(CS_2)$	$M^+(CS_2)_2$	$M^+(CS_2)_3$
Ca^+	≥2.6 × 10^5 (≤−7.4)	8.4 × 10^6 (−9.4)	5.0 × 10^6 (−9.1)
V^+	≥3.4 × 10^6 (≤−8.9)	1.3 × 10^8 (−11.1)	
Cr^+	≥7.4 × 10^5 (≤−8.0)	4.4 × 10^7 (−10.4)	
Mn^+	≥6.1 × 10^4 (≤−6.5)	≥2.9 × 10^7 (≤−10.2)	
Fe^+	≥2.4 × 10^6 (≤−8.7)	≥3.9 × 10^8 (≤−11.7)	
Co^+	≥6.7 × 10^6 (≤−9.3)	≥2.6 × 10^8 (≤−11.5)	5.2 × 10^5 (−7.8)
Ni^+	≥9.6 × 10^6 (≤−9.5)	8.1 × 10^7 (−10.8)	1.4 × 10^7 (−9.7)
Cu^+	≥6.8 × 10^6 (≤−9.3)	1.3 × 10^8 (−11.0)	
Zn^+	1.1 × 10^6 (−8.2)	1.3 × 10^8 (−8.4)	
Ga^+	1.2 × 10^5 (−6.9)		
Ge^+	≥2.5 × 10^7 (≤−10.1)	8.4 × 10^5 (−8.1)	
Se^+	≥1.8 × 10^8 (≤−11.2)		
Sr^+	≥5.7 × 10^5 (≤−7.8)	3.4 × 10^6 (−8.9)	7.6 × 10^5 (−8.0)
Mo^+	≥8.4 × 10^6 (≤−9.4)	≥3.4 × 10^8 (≤−11.6)	9.5 × 10^6 (−9.4)
Ru^+	≥5.9 × 10^6 (≤−9.2)	≥7.5 × 10^7 (≤−10.7)	≥2.6 × 10^8 (≤−11.4)
Rh^+	≥2.5 × 10^6 (≤−8.7)	≥7.9 × 10^7 (≤−10.8)	9.2 × 10^7 (−10.9)
Pd^+	≥3.4 × 10^6 (≤−8.9)	≥4.2 × 10^7 (≤−10.3)	2.8 × 10^7 (−10.5)
Ag^+	≥1.1 × 10^6 (≤−8.2)	3.9 × 10^7 (−10.3)	
Cd^+	5.1 × 10^5 (−7.8)	6.5 × 10^5 (−7.9)	
In^+	7.5 × 10^4 (−6.7)		
Sn^+	7.8 × 10^5 (−8.0)		
Te^+	1.2 × 10^6 (−7.9)		
Ba^+	≥1.2 × 10^7 (≤−9.6)	4.7 × 10^5 (−7.7)	
Re^+	≥3.3 × 10^7 (≤−10.2)	≥ 2.1 × 10^8 (≤−11.3)	
Os^+	≥4.9 × 10^7 (≤−10.5)	≥1.0 × 10^9 (≤−12.5)	
Ir^+	≥5.9 × 10^7 (≤−10.6)	≥1.1 × 10^9 (≤−12.3)	6.7 × 10^6 (−9.3)
Pt^+	≥3.8 × 10^7 (≤−10.3)	≥ 2.8 × 10^9 (≤−12.9)	6.4 × 10^6 (−9.3)
Au^+	≥ 1.7 × 10^7 (≤−9.8)	≥ 1.7 × 10^9 (≤−12.6)	
Tl^+	8.0 × 10^4 (−6.6)		
Pb^+	1.2 × 10^5 (−6.9)		
Bi^+	1.4 × 10^5 (−7.0)		

[a] The standard free energy changes, $\Delta G°$ (kcal mol^{-1}) = $-RT \ln K$, are given in parentheses and have an uncertainty estimated to be no more than 0.3 kcal mol^{-1}.

contribute to the increased lifetime of the intermediate that causes the observed increase in rate.

3.8. Equilibrium Kinetics and Standard Free Energies of Association. Equilibrium analyses performed on the kinetic results indicate that equilibrium is attained in many of the CS_2 addition reactions. These analyses are based on plots of product-to-reactant ion signal ratios as a function of CS_2 flow. Equilibrium is achieved when this plot achieves linearity, viz. when $[M^+(CS_2)_n]/[M^+(CS_2)_{n-1}] = K[CS_2]$. The equilibrium kinetics for the association reactions that were observed was well behaved. The ion-signal ratio plots were nicely linear. This is demonstrated in Figure 6 for the sequential addition of two CS_2 molecules to Zn^+. Table 6 lists the equilibrium constants that were measured for the addition of up to 3 molecules of CS_2 to various M^+ ions. Also included are the standard free energies of association derived from $\Delta G° = -RT \ln K$ at 295 ± 2 K. They have values in the range from −6.7 to <−12.9 kcal mol^{-1}.

Table 7 lists the equilibrium constants measured for the addition of up to three molecules of CS_2 to MS^+ and MS_2^+ ions at 295 ± 2 K. Also included are the corresponding values for the standard free energy change, $\Delta G°$.

3.9. Periodic Trends in the Efficiency and Standard Free Energy for CS_2 Ligation of M^+. The standard free energies for CS_2 addition that are reported in Tables 6 and 7 are generally unknown from previous measurements or calculations, as far as we are aware. Figure 7 explores the periodic variation in the values of the measured efficiencies and the standard binding free energies derived from the equilibrium constant measurements (see Table 6) for the additions of CS_2 to M^+ observed at 295 ± 2 K. There is a clear periodic correspondence in the

TABLE 7: Equilibrium Constants, *K* (Standard State = 1 atm), Measured for Sequential CS_2 Addition to MS^+ and MS_2^+ at 295 ± 2 K[a]

	K (Δ*G*°)		
MS_n^+	$MS_n^+(CS_2)$	$MS_n^+(CS_2)_2$	$MS_n^+(CS_2)_3$
ScS^+	≥1.1 × 10^7 (≤−9.6)	≥6.0 × 10^7 (≤−10.6)	6.5 × 10^7 (−10.7)
TiS^+	≥1.4 × 10^7 (≤−9.7)	≥2.3 × 10^8 (≤−11.4)	
AsS^+	2.5 × 10^5 (−7.4)		
SeS^+	1.4 × 10^6 (−8.4)		
YS^+	≥4.5 × 10^6 (≤−9.1)	≥5.3 × 10^7 (≤−10.5)	6.6 × 10^7 (10.7)
ZrS^+	≥7.5 × 10^7 (≤−10.7)	≥6.5 × 10^7 (≤−10.6)	3.9 × 10^7 (10.3)
NbS^+	8.4 × 10^6 (−9.4)	≥2.4 × 10^9 (≤−12.7)	
NbS_2^+	≥4.9 × 10^7 (≤−10.5)	≥1.7 × 10^{11} (≤−15.3)	3.4 × 10^5 (−7.5)
LaS^+	≥1.5 × 10^6 (≤−8.4)	7.5 × 10^6 (−9.4)	6.6 × 10^6 (−9.3)
HfS^+	≥4.3 × 10^7 (≤−10.4)	1.1 × 10^8 (−10.9)	3.8 × 10^7 (−10.3)
TaS^+	8.4 × 10^6 (≤−9.4)	≥6.5 × 10^8 (≤−12.0)	
TaS_2^+	≥5.4 × 10^7 (≤−10.5)	≥2.0 × 10^9 (≤−12.7)	8.4 × 10^5 (−8.1)
WS_2^+	≥3.0 × 10^8 (≤−11.5)	≥3.3 × 10^7 (≤−10.2)	
ReS^+	≥ 1.6 × 10^{10} (≤−13.9)	≥1.0 × 10^9 (≤−12.3)	
OsS^+	8.6 × 10^7 (−10.8)		

[a] The standard free energy changes, $\Delta G°$ (kcal mol^{-1}), are given in parentheses and have an uncertainty estimated to be no more than 0.3 kcal mol^{-1}.

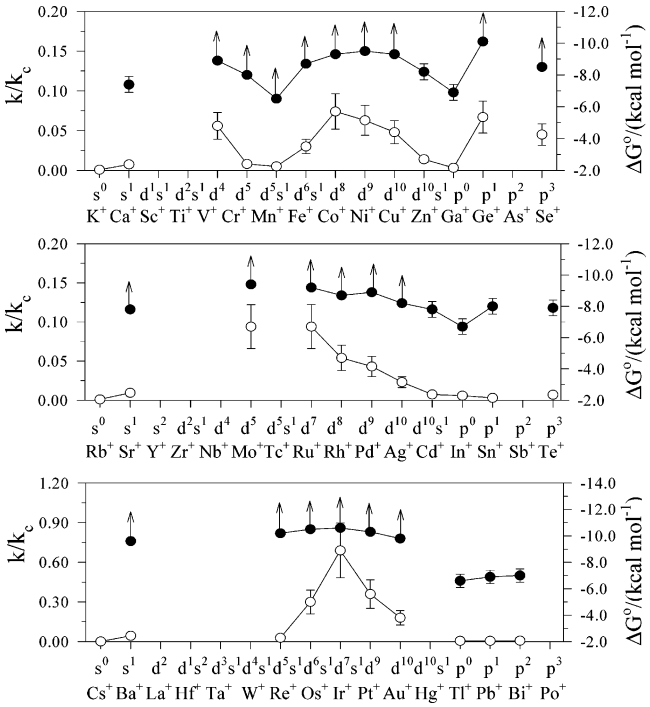

Figure 7. Variations observed in the efficiency (open circles), (k/k_c), and the standard free energy change (solid circles) for CS_2 addition with the electron configuration of the bare atomic cations.

trends in reaction efficiency and standard binding free energy across the three periods of the periodic table.

In analogy with the binding free energies of M^+-CO_2 that we have discussed previously,[21] the M^+-CS_2 binding free energies across the first row of the periodic table are expected to be determined primarily by the trend in electrostatic attraction (the binding energy or enthalpy) because large variations in the entropy change are not expected. The trend in electrostatic attraction follows the trend in ion size and the trend in repulsion between the metal d orbitals and the occupied orbitals of CS_2, the order of repulsion being $3d\sigma > 3d\pi > 3d\delta$. Minima in D_0 or $\Delta G°$ appear for $Mn^+(3d^54s^1)$ and $Ga^+(3d^{10}4s^24p^0)$ where the repulsion is largest. The increase in M^+-CS_2 attraction due to decreasing size determines the trend in increasing bond energy observed just beyond Mn^+ and Ga^+ and also beyond In^+.

3.10. Comparison of the Atomic-Metal Ion Chemistry of CO_2 and CS_2. Reactions of atomic cations with CO_2 have been previously investigated in our laboratory using the same technique as employed here.[21] A comparison with results reported here for CS_2 indicates that these two molecules exhibit both similarities and differences in their reactivities toward atomic-metal cations. Generally speaking, they both react with early transition-metal cations by X-atom (X = O, S) transfer and react with late transition and main-group metal cations by CX_2 addition. The reactions with CS_2 are generally more efficient.

Not surprisingly, group 1 (s^0) cations, which have a rare-gas configuration, are nonreactive with both CO_2 and CS_2. The group 2 cations add CS_2 with rates at least 20 times those observed with CO_2, and this can be attributed to the stronger electrostatic interaction expected with CS_2 because the polarizability of CS_2 (8.74×10^{-24} cm^3) is 3 times that of CO_2 (2.911×10^{-24} cm^3).[32]

Transfer of O from CO_2 and S from CS_2 is seen with early transition-metal cations in the fourth period (groups 3 and 4), in the fifth period (groups 3−5), and in the sixth period (groups 3−6), but further along the sixth period with CS_2. Re^+ and Os^+ abstract an S atom from CS_2 but not an O atom from CO_2. S atom transfer from CS_2, which occurs at or close to every collision, is strikingly more efficient than O atom transfer from CO_2: by a factor of 10 in the fourth period, often by a factor of more than 2 in the fifth and sixth period, and by a factor of 10 in the reaction with W^+.

The group 15 (p^2) cations As^+ and Sb^+ and the group 16 (p^3) cation Se^+ abstract an S atom from CS_2 but do not abstract an O atom from CO_2, as expected from the appropriate O-atom and S-atom affinities, at least to the extent that these are known. CS_2 transfers an electron to Hg^+ with unit efficiency whereas CO_2 does not. Thermodynamics is again in control because the transfer of an electron from CS_2 is exothermic by 0.37 eV and from CO_2 is endothermic by 3.33 eV.

Higher-order molecule addition and atom transfer generally are favored with CS_2.

4. Conclusions

Our measurements of equilibrium and nonequilibrium kinetics, product distributions, and higher-order chemistry demonstrate that CS_2 shows a high reactivity toward positively charged atomic centers. The experimental survey of CS_2 reactivity with 46 atomic cations along and down the periodic table has characterized periodicities in reactivity along three periods of the periodic table. The early transition-metal cations including W^+, Re^+ and Os^+ are the best S-atom acceptors along with the main-group cations As^+, Se^+ and Sb^+. The other atomic cations, particularly the group 8 and 9 cations, generally are favorable centers for $M^+(CS_2)_n$ cluster formation with Ru^+, Rh^+, Os^+ and Ir^+ bonding sequentially with up to four CS_2 molecules at the room-temperature conditions of our ICP/SIFT instrument. Addition of CS_2 to sixth-period atomic ions is particularly effective, presumably because of strong bonding interactions that perhaps are a consequence of metal-ion insertion. CS_2 also has been found to be an efficient electron donor to Hg^+.

Secondary and higher-order reactions lead to further S-atom abstraction with Y^+, Zr^+, Nb^+, Hf^+, Ta^+, W^+, Re^+ and Os^+ to form disulfide cations and with Ta^+ to form TaS_3^+. Further CS_2 addition was observed to occur with the cations MCS_2^+, MS^+, MS_2^+, CS_2^+, TaS_3^+ to form $M^+(CS_2)_n$ ($n \leq 4$), $MS^+(CS_2)_n$ ($n \leq 4$), $MS_2^+(CS_2)_n$ ($n \leq 3$), $(CS_2)_2^+$ and $TaS_3^+(CS_2)$. Up to four CS_2 molecules were observed to add sequentially to bare metal cations and monosulfide cations, and three to disulfide cations.

Variations in the standard free energy changes for CS_2 ligation that were determined from equilibrium constant measurements are consistent with what is expected from the variation in electrostatic attraction between M^+ and CS_2. The latter follows the trend in atomic-ion size and the trend in repulsion between the d orbitals of the atomic cations and the occupied orbitals of CS_2.

Acknowledgment. Continued financial support from the Natural Sciences and Engineering Research Council of Canada is greatly appreciated. Also, we acknowledge support from the National Research Council, the Natural Science and Engineering Research Council and MDS SCIEX in the form of a Research Partnership grant. As holder of a Canada Research Chair in Physical Chemistry, D.K.B. thanks the contributions of the Canada Research Chair Program to this research.

References and Notes

(1) Stiefel, E. I., Matsumoto, K., Eds. *Transition Metal Sulfur Chemistry*; ACS Symposium Series 653; American Chemistry Society: Washington, DC, 1996.
(2) Hua, M.; Garcia, C. I.; DeArdo, A. J. *Metall. Mater. Trans. A* **1997**, *28A*, 1769.
(3) Morita, M.; Hosoya, Y. *Mech. Work. Steel Process. Conf. Proc.* **1998**, *35*, 185.
(4) Ibers, J. A. *Chem. Soc. Rev.* **1982**, *11*, 57.
(5) Pandey, K. K. *Coord. Chem. Rev.* **1995**, *140*, 37.
(6) Butler, I. S.; Fenster, A. E. *J. Organomet. Chem.* **1974**, *66*, 161.
(7) Huber, H.; Ozin, G. A.; Power, W. J. *Inorg. Chem.* **1977**, *16*, 2234.
(8) Zhou, M.; Andrews, L. *J. Phys. Chem. A* **2000**, *104*, 4394.
(9) Zeng, A.; Kong, Q.; Wang, Y.; Zhou, M. *Chem. Phys.* **2003**, *292*, 111.
(10) Rue, C.; Armentrout, P. B.; Kretzschmar, I.; Schröder, D.; Harvey, J. N.; Schwarz, H. *J. Chem. Phys.* **1999**, *110*, 7858.
(11) Papai, I.; Hannachi, Y.; Gwizdala, S.; Mascetti, J. *J. Phys. Chem. A* **2002**, *106*, 4181.
(12) Armentrout, P. B.; Beauchamp, J. L. *Chem. Phys.* **1980**, *50*, 27.
(13) Kretzschmar, I.; Schröder, D.; Schwarz, H.; Rue, C.; Armentrout, P. B. *J. Phys. Chem. A* **2000**, *104*, 5046.
(14) Kretzschmar, I.; Schröder, D.; Schwarz, H.; Rue, C.; Armentrout, P. B. *J. Phys. Chem. A* **1998**, *102*, 10060.
(15) Rue, C.; Armentrout, P. B.; Kretzschmar, I.; Schröder, D.; Schwarz, H. *Int. J. Mass Spectrom.* **2001**, *210/211*, 283.
(16) Rue, C.; Armentrout, P. B.; Kretzschmar, I.; Schröder, D.; Schwarz, H. *J. Phys. Chem. A* **2001**, *105*, 8456.
(17) Schroeder, D.; Kretzschmar, I.; Schwarz, H.; Rue, C.; Armentrout, P. B. *Inorg. Chem.* **1999**, *38*, 3474.
(18) Rue, C.; Armentrout, P. B.; Kretzschmar, I.; Schroeder, D.; Schwarz, H. *J. Phys. Chem. A* **2002**, *106*, 9788.
(19) Kretzschmar, I. Energetics and Reactivity of the Binary Transition-Metal Sulfides of the 3rd and 4th Row. Dissertation TU Berlin, Aachen: Shaker Verlag: 1999 (ISBN 3-8265-6294-1).
(20) Jiang, N.; Zhang, D. *Chem. Phys. Lett.* **2002**, *366*, 253.
(21) Koyanagi, G. K.; Bohme, D. K. *J. Phys. Chem. A* **2006**, *110*, 1232.
(22) Mackay, G. I.; Vlachos, G. D.; Bohme, D. K.; Schiff, H. I. *Int. J. Mass Spectrom. Ion Phys.* **1980**, *36*, 259.
(23) Raksit, A. B.; Bohme, D. K. *Int. J. Mass Spectrom. Ion Processes* **1983**, *55*, 69.
(24) Koyanagi, G. K.; Lavrov, V. V.; Baranov, V.; Bandura, D.; Tanner, S.; McLaren, J. W.; Bohme, D. K. *Int. J. Mass Spectrom.* **2000**, *194*, L1.
(25) Koyanagi, G. K.; Baranov, V. I.; Tanner, S. D.; Bohme, D. K. *J. Anal. At. Spectrom.* **2000**, *15*, 1207.
(26) Moore, C. E. *Atomic energy levels as derived from the analyses of optical spectra*; U.S. National Bureau of Standards: Washington, DC, 1971.
(27) Van Kleef, T. A. M.; Metsch, B. C. *Physica B+C: Physics of Condensed Matter + Atomic, Molecular and Plasma Physics, Optics (Amsterdam)* **1978**, *95*, 251.
(28) Lavrov, V. V.; Blagojevic, V.; Koyanagi, G. K.; Orlova, G.; Bohme, D. K. *J. Phys. Chem. A* **2004**, *108*, 5610.
(29) Condon, E. U.; Shortley, G. H. *The theory of atomic spectra*; Cambridge University Press: Cambridge, U.K., 1963.
(30) Garstang, R. H. *Mon. Not. R. Astron. Soc.* **1962**, *124*, 321.

(31) Su, T.; Chesnavich, W. J. *J. Chem. Phys.* **1982**, *76*, 5183.
(32) Lide, D. R. *CRC Handbook of Chemistry and Physics*, 82nd ed.; CRC Press: Boca Raton, FL, 2001.
(33) Cheng, P.; Koyanagi, G. K.; Bohme, D. K. Manuscript in preparation.
(34) Lias, S. G.; Bartmess, J. E.; Liebman, J. F.; Holmes, J. L.; Levin, R. D.; Mallard, W. G. *J. Phys. Chem. Ref. Data, Suppl.* **1988**, *17*, 861.
(35) Armentrout, P. B. *Int. J. Mass Spectrom.* **2003**, *227*, 289.
(36) Luo, Y.; Wan, X.; Ito, Y.; Takami, S.; Kubo, M.; Miyamoto, A. *Chem. Phys.* **2002**, *282*, 197.
(37) Baranov, V.; Bohme, D. K. *Int. J. Mass Spectrom. Ion Processes* **1996**, *154*, 71.
(38) Kretzschmar, I.; Schröder, D.; Schwarz, H.; Armentrout, P. B. *Int. J. Mass Spectrom.* **2003**, *228*, 439.